# Effects of Channel Rotation on Turbulent Boundary Layers along a Convex Surface*

Koji KIKUYAMA**, Takao MAEDA***,
Kenji NISHIBORI**** and Satoshi NOMURA*****

Effects of the centrifugal force due to wall curvature and the Coriolis force due to system rotation on turbulent boundary layers along a convex surface are studied experimentally using a curved channel of a constant cross-section rotating about an axis perpendicular to the main flow. Time-averaged and turbulent components of the velocities inside the channel were measured using hot wire probes during the channel rotation. Besides wall curvature, channel rotation was found to have a large effect on stabilization or destabilization of the turbulent motion in the boundary layer. Stabilizing effects appear more dominant on the suction side, and the flow tends to become laminarized there. When the Coriolis force acts toward the convex surface resulting in higher pressure on that side, the destabilizing effects due to the force cancel the stabilizing effects of the centrifugal force, and the velocity profiles are almost unchanged in the downstream direction. Comparison was made with the turbulence behavior on the concave surface in the same channel.

***Key Words***: Boundary Layer, Turbulence, Coriolis Force, Convex Surface, Velocity Distribution

## 1. Introduction

It is necessary to clarify the details of the nature of flow in the impeller passages of turbomachines in order to obtain higher efficiencies. The flows in the impeller passages are, however, very complicated because they are subject to the centrifugal and Coriolis forces generated by wall curvature and system rotation, respectively. Though many studies have been conducted on the channel flows dominated by external forces such as the centrifugal and Coriolis forces[1]-[3], few studies have reported the composite effects of the centrifugal and Coriolis forces on the flow[4]. In this study, the time-averaged and turbulent components of velocities have been measured along the convex surface, and the Monin-Oboukhov formula was examined in relation to the gradient Richardson numbers for wall curvature and channel rotation. Comparison was also made with the flows in the boundary layer along the concave surface[5].

## 2. Nomenclature

$A, B$ : constants of Eq.(8)
$C_p$ : static pressure coefficient, $(p-p_0)/(\rho U_m^2/2)$
$D$ : channel width $=30$ mm
$h$ : channel height $=120$ mm
$H$ : shape factor, $\delta_1/\delta_2$
$k_c$ : inverse of surface curvature, $1/R$
$l$ : mixing length, $\sqrt{-\overline{uv}}/(\partial U/\partial y_1)$
$l_0$ : mixing length along flat plate for stationary state
$N$ : rotation number, $\Omega D/U_m$ (Eq.(7))
$N_{\delta_2}$ : local rotation number, $\Omega\delta_2/U_e$
$p$ : pressure
$p_0$ : pressure measured at section S-1
$R$ : surface curvature $=185$ mm
$Re$ : Reynolds number $=10\,000$
$Ri_c, Ri_r$ : gradient Richardson numbers (Eqs.(3)

* Received 17th March, 1992. Paper No. 90-1405A
** Faculty of Engineering, Nagoya University, Furo-cho, Chikusa-ku, Nagoya 464-01, Japan
*** Faculty of Engineering, Mie University, Kamihama-cho, Tsu, Mie 514, Japan
**** Faculty of Engineering, Daido Institute of Technology, 2-21 Minami-ku, Nagoya 457, Japan
***** Toshiba Corporation, 1385 Otawara, Tochigi 329-26, Japan

and (4))

$u, v, w$ : turbulent velocity components in $x$, $y$ and $z$ directions

$U, V, W$ : time-averaged velocity components in $x$, $y$ and $z$ directions

$U_e$ : external flow velocity

$U_m$ : bulk mean velocity

$U_\tau$ : friction velocity

$x, y, z$ : coordinates in rotating channel

$y_1$ : distance from convex surface

$\beta_c, \beta_r$ : constants of Eq.(6)

$\delta$ : boundary layer thickness

$\delta_1$ : displacement thickness

$\delta_2$ : momentum thickness

$\Omega$ : angular velocity of channel

Subscripts

$c$ : channel curvature

$r$ : channel rotation

## 3. Experimental Apparatus and Procedure

Figure 1 shows the schematic outline of the experimental apparatus. The test channel is mounted on a rotating disk. Air is introduced to the test section through the chamber, the honeycomb and nozzle, successively, and is then discharged by a fan.

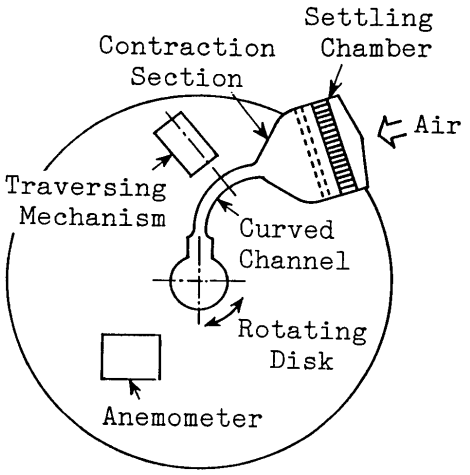


Fig. 1 Rotating disk and channel

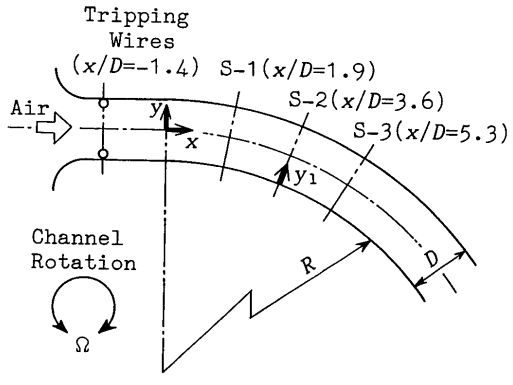


Fig. 2 Configuration of channel

The configuration of the rotating channel is shown in Fig. 2. It has a radius of surface curvature of $R=185$ mm, and has a constant cross-section. The width and height of the channel are 30 mm and 120 mm, respectively. The boundary layer in the inlet region of the channel is made turbulent by a tripping wire of 1.5 mm diameter, as shown in Fig. 2. Measurements are made at the sections of S-1 ($x/D=1.9$), S-2 ($x/D=3.6$) and S-3 ($x/D=5.3$) downstream from the starting section of curvature, and the probes are traversed at the mid-height of $z=0$.

The hot wire anemometer and traversing unit of the probe are mounted on the rotating disk. The traverse of the hot wire probe is conducted by a stepping motor on the disk and controlled by a small computer in the stationary system. The output from the anemometer is transmitted to the stationary system by means of slip rings, while the static pressure on the channel walls is measured in the pressure tappings and transmitted to the stationary system through the mechanical seals.

Experiments were carried out under the constant Reynolds number of $Re=10^4$ and the rotation numbers of $N(=\Omega D/U_m)=0$, $\pm0.075$ and $\pm0.15$, where the positive or negative sign corresponds to the rotational direction of the channel.

## 4. Equations

### 4.1 Velocity profile of potential core

As the vorticity of the potential core in a channel rotating with an angular velocity of $\Omega$ is equal to $2\Omega$, the velocity profile in the core is given by

$$U_p=C_1/r-\Omega r. \tag{1}$$

When $r=R+y_1$ and $k_c=1/R$, Eq.(1) is replaced by

$$U_p=C/(1+k_c y_1)-\Omega(1+k_c y_1)/k_c. \tag{2}$$

In the calculation of the boundary layer thickness, $U_p$ given by Eq.(2) was used as the velocity outside the boundary layer, and the values of $k_c$ were determined to be $0.18/D$ and $0.34/D$ by the experimental results of the velocity profile.

### 4.2 Gradient Richardson numbers

From the analogy between the Coriolis and centrifugal forces acting on the turbulent motions, the following gradient Richardson numbers are given by Bradshaw[6]. For the centrifugal force:

$$Ri_c=(2U/r^2)(\partial Ur/\partial y_1)/(\partial U/\partial y_1)^2 \tag{3}$$

and for the Coriolis force:

$$Ri_r=-2\Omega(\partial U/\partial y_1-2\Omega)/(\partial U/\partial y_1)^2. \tag{4}$$

In the curved duct $Ri_c$ takes a negative value on the concave side and a positive value on the convex side, and in the rotating duct $Ri_r$ becomes negative on the higher pressure side, and vice versa. When the value of the Richardson number is positive in the boundary

layer, the turbulence energy is decreased.

Bradshaw[6] extended the Monin-Oboukhov formula according to the analogy between the buoyancy and the Coriolis force, and presented the expression for the relation between the mixing length $l$ and the Richardson number $Ri$,

$$l/l_0=1-\beta Ri \quad (5)$$

where $l_0$ denotes the value of $l$ on the flat plate at the stationary state. The values of $\beta$ are suggested as $\beta=7\sim10$ on the convex surface by Bradshaw and $\beta=6\pm2$ for the rotating flat surface by Johnston[7]. If the effects of the centrifugal and the Coriolis forces on the mixing length are assumed by the linear relation, the Monin-Oboukhov formula can be modified as follows.

$$l/l_0=1-\beta_c Ri_c-\beta_r Ri_r \quad (6)$$

where $Ri_c$ and $Ri_r$ are the gradient Richardson numbers due to the surface curvature and system rotation, respectively.

In order to express the relative effects of the Coriolis force, a dimensionless rotation parameter $N$ is defined by the following equation as

$$N=\Omega D/U_m \quad (7)$$

where $\Omega$ is taken to be positive when the Coriolis force acts toward the convex surface and vice versa.

## 5. Experimental Results and Discussion

### 5.1 Changes in static pressure

Figure 3 shows the changes in the static pressure along the convex surface. The pressure is made dimensionless by taking the difference from that in section S-1 and is plotted along the flow. The pressure change on the concave surface for the stationary state ($N=0$) is also shown for reference. For the stationary state ($N=0$), the pressure decreases at an almost constant rate from section S-1 to S-3 ($0.0<x/D\leq5.3$). When the channel rotates, the pressure decrease is promoted on the pressure side ($N>0$) but suppressed on the suction side due to the destabilizing and stabilizing effects of the Coriolis force, respectively. Compared with the pressure change on the concave surface, the changes on the convex surface are lessened largely due to the stabilizing effects of the centrifugal force caused by wall curvature.

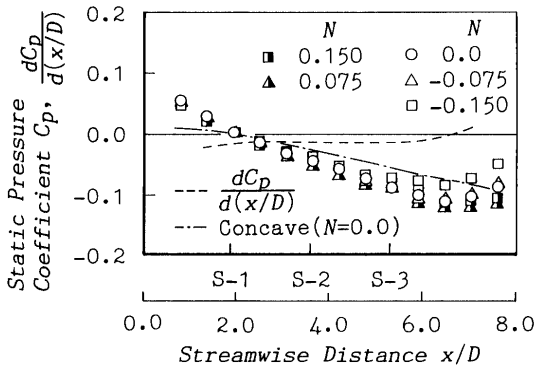


Fig. 3 Plots of static pressure coefficient

### 5.2 Time-averaged velocity distributions

In order to examine the effects of the end walls on the flow near the mid-height of the channel, the time-averaged velocity and turbulence intensity along the $z$-axis were measured at $y_1=5$ mm ($y_1/\delta=0.48$) in section S-3 as shown in Fig. 4. Both the profiles of the time-averaged velocity and the turbulence intensity are almost uniform in the region of $-0.3<z/h<0.3$, regardless of the rotation number $N$.

Figure 5 presents the time-averaged velocity profiles measured in sections S-1 and S-3 for the various rotational speeds. In section S-1 the velocity distributions exhibit almost the same profiles for different rotation numbers, but in section S-3 the velocity gradient near the wall increases slightly with the increase in $N$.

### 5.3 Turbulence intensities and Reynolds shear stress

The turbulence intensities $\sqrt{\overline{u^2}}$, $\sqrt{\overline{v^2}}$ and $\sqrt{\overline{w^2}}$ for the various rotational speeds at sections S-1 and S-3 are shown in Figs. 6(a) and (b), respectively. In section S-1 the turbulence intensities for $N>0$ are

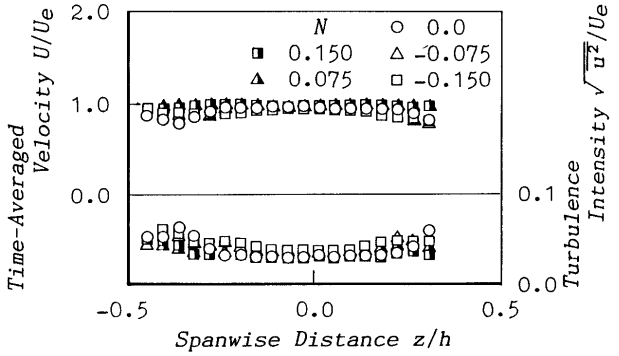


Fig. 4 Time-averaged velocity and turbulence intensity profiles along $z$-axis

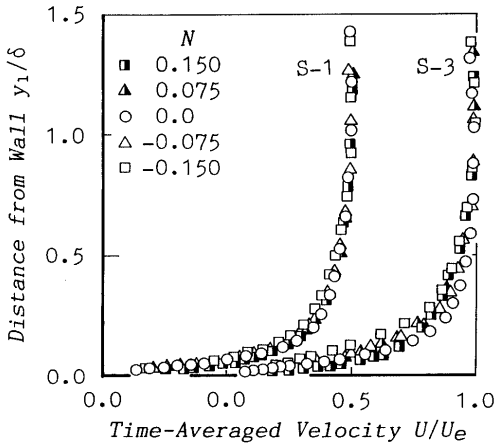


Fig. 5 Time-averaged velocity profiles

increased near the convex wall due to the destabilizing effects of the Coriolis force.

The effects of the channel rotation and the wall curvature seem to be dominant in section S-3, where

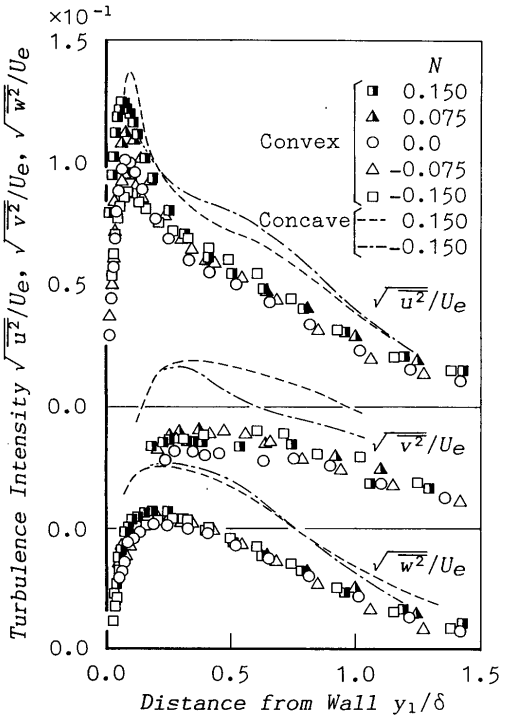


Fig. 6(a) Turbulence intensities profiles in upstream section S-1

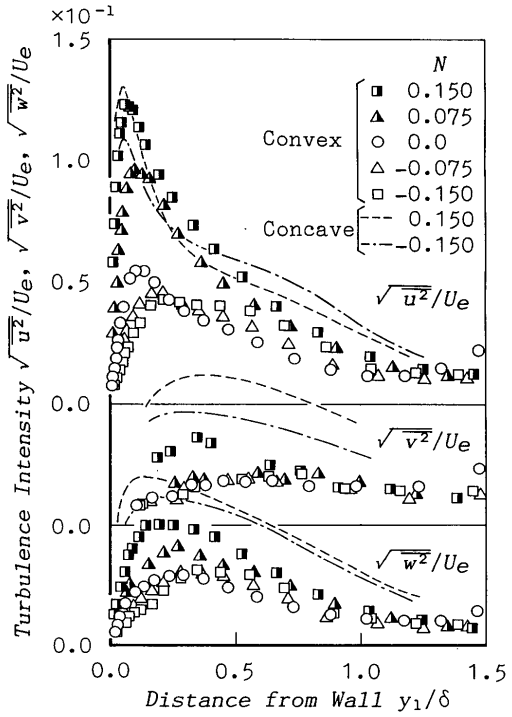


Fig. 6(b) Turbulence intensities profiles in downstream section S-3

the values of $\sqrt{\overline{u^2}}$, $\sqrt{\overline{v^2}}$ and $\sqrt{\overline{w^2}}$ are largely decreased due to the stabilizing effects of wall curvature when $N=0$ and they are further decreased with the channel rotation of $N<0$. Compared with the concave surface for $N=\pm 0.15$, the turbulence intensities on the convex surface exhibit smaller values due to the suppression of the turbulent motion due to the centrifugal force.

The Reynolds shear stress along the convex surface is shown for the various rotational speeds in Fig. 7. The value of $-\overline{uv}/U_e^2$ for $N<0$ tends to be almost zero due to both the stabilizing effects of both the Coriolis and centrifugal forces. The distribution of $-\overline{uv}/U_e^2$ is similar to those of the turbulence intensities.

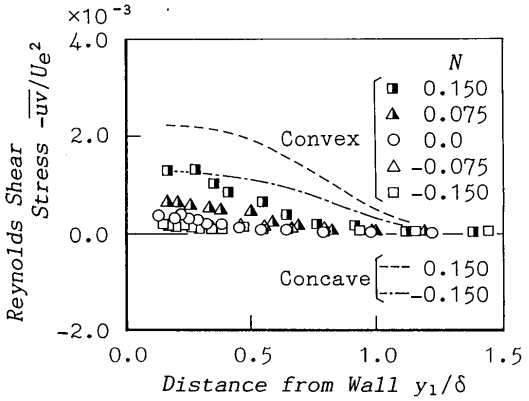


Fig. 7 Reynolds shear stress profiles in downstream section S-3

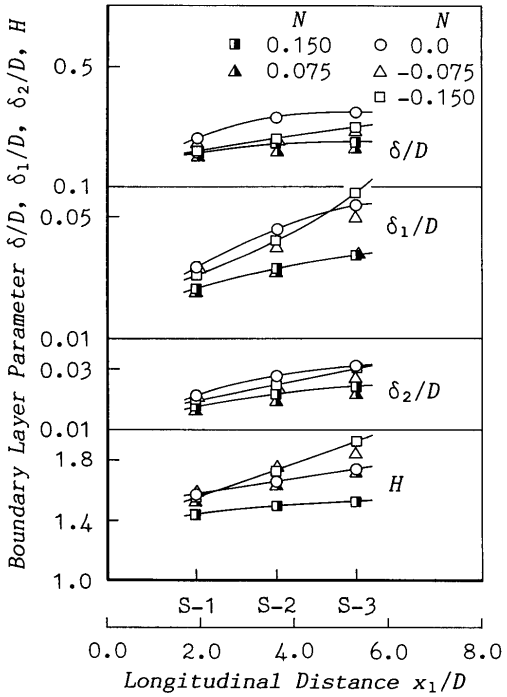


Fig. 8 Boundary layer parameters

### 5.4 Boundary layer parameters

Figure 8 shows the streamwise changes in the boundary layer thickness $\delta$, the displacement thickness $\delta_1$, the momentum thickness $\delta_2$ and the shape factor $H(=\delta_1/\delta_2)$. The boundary layer thickness $\delta$ takes smaller values for $N>0$ because the velocity gradient near the wall for $N>0$ increases due to the destabilizing effects of the Coriolis force. On the other hand, the boundary layer for $N<0$ increases due to the stabilizing effects of the Coriolis force and the secondary flows generated in the channel.

The displacement thickness and the momentum thickness exhibit almost the same changes as the boundary layer thickness. The increments in $\delta_1$ in the downstream direction for $N\leq 0$ are larger than those for $N>0$.

The shape factor for $N<0$ takes a larger value than that for the stationary state. The value of $H$ in section S-3 for $N<0$ is almost equal to 1.8, which lies in the range of the turbulent separation on a flat plate. The relaminarization of the flow, however, suppresses the separation since the laminar boundary layer separates at a larger value of $H=3.5$.

### 5.5 Logarithmic velocity distributions

To compare the nature of the turbulent flow on the convex surface with that on a flat plate with no pressure gradient, the logarithmic relationship between $U/U_\tau$ and $y_1U_\tau/\nu$, given by the following equation is examined in Fig. 9.

$$U/U_\tau=A+B\log(y_1U_\tau/\nu) \qquad (8)$$

where $U_\tau$ is the frictional velocity which is obtained from the Preston tube measurement. In the same figure the curves of $U/U_\tau$ both for the turbulent and viscous regions on a flat plate are also plotted. Few differences can be seen in the logarithmic velocity distribution in the upstream section S-1 when the rotational speed is changed. In section S-3, however, the viscous layer seems to be thicker and exhibits a laminar flow nature when $N$ is negative. On the other hand, the curve for $N=0.15$ tends to approach that for the flat plate.

The changes in the constants $A$ and $B$ in Eq. (8) divided by the values for the stationary state are shown against the rotation number $N_{\delta_2}(=\Omega\delta_2/U_e)$ in Fig. 10. The value of $A/A_0$ for $N_{\delta_2}>0$ decreases below 1.0 with increasing $N_{\delta_2}$.

The value of $B/B_0$ decreases with increasing $N_{\delta_2}$ and the linear relationship between $B/B_0$ and $N_{\delta 2}$ is obtained in the range $-0.004<N_{\delta_2}<0.0035$ as follows.

$$B/B_0=-66.1N_{\delta_2}+1. \qquad (9)$$

In the previous paper[5] almost the same expression is obtained on the concave surface as $B/B_0=-42.3N_{\delta_2}+1$.

### 5.6 Mixing lengths

In order to examine the effects of the centrifugal and the Coriolis forces on the mixing length, the ratio of the Richardson numbers given by Eqs. (3) and (4) is shown in Fig. 11. $Ri_r/Ri_c$ takes negative values when $N>0$ and is positive when $N<0$. The values of $|Ri_r/Ri_c|$ are large near the wall where the effects of Coriolis force can be seen to be dominant. $|Ri_r/Ri_c|$ for $N>0$ decreases with the distance away from the wall and tends to be zero outside the boundary layer, while $|Ri_r/Ri_c|$ for $N<0$ approaches a constant value with increasing distance from the wall.

Figure 12 shows the mixing length $l=\sqrt{-\overline{uv}}/(\partial U/\partial y_1)$ on the convex surface. The mixing length along the flat plate for the stationary state is also indicated in the figure. The mixing lengths on the

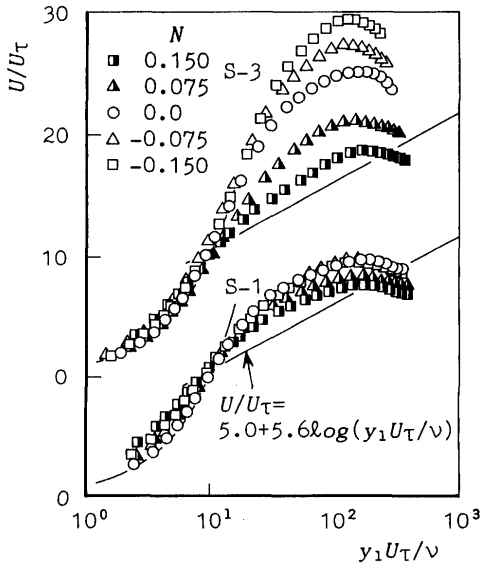


Fig. 9 Logarithmic velocity distributions

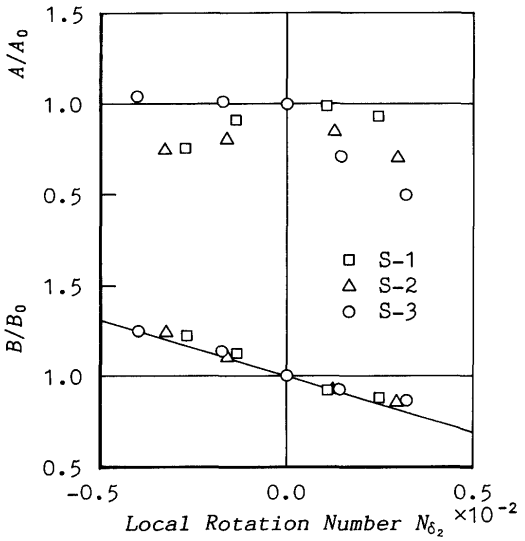


Fig. 10 Changes in $A/A_0$ and $B/B_0$

convex surface has smaller values than those on a flat plate due to the effects of wall curvature, regardless of the rotational speed. Compared with that in the stationary state, the mixing length increases on the pressure side due to channel rotation.

As the centrifugal and Coriolis forces act in the present rotating curved channel, the Monin-Oboukhov formula for the stationary curved channel is revised and the ratio of the mixing lengths is assumed to be given by a linear relationship of Richardson numbers as Eq.(6). With the use of the experimental data in section S-3, the values of $\beta_c$ and $\beta_r$ are calculated to be approximately 6.1 and 2.8, respectively. In order to check the validity of Eq.(6) the changes in $(l/l_0)_c$ and $(l/l_0)_r$ defined by the following equations are plotted in Figs. 13(a) and (b):

$$(l/l_0)_c = l/l_0 + \beta_r Ri_r \quad (\beta_r = 2.8) \tag{10}$$

$$(l/l_0)_r = l/l_0 + \beta_c Ri_c \quad (\beta_c = 6.1). \tag{11}$$

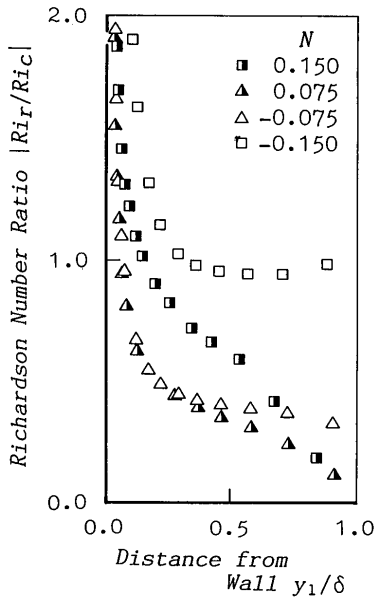


Fig. 11 Ratio $Ri_c$ and $Ri_r$

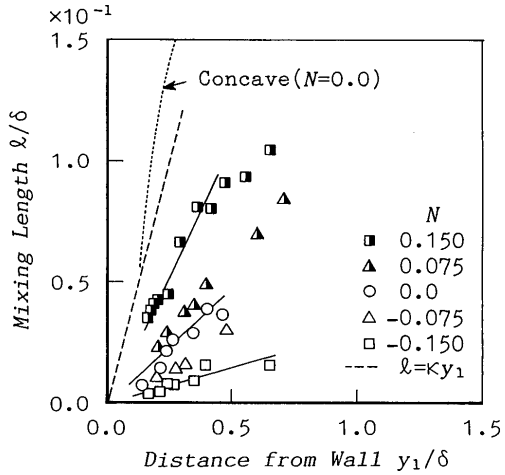


Fig. 12 Plots of mixing length versus distance from wall

In the same figures the following relationships obtained from Eq.(6) are also plotted.

$$(l/l_0)_c = 1 - \beta_c Ri_c \quad (\beta_c = 6.1) \tag{12}$$

$$(l/l_0)_r = 1 - \beta_r Ri_r \quad (\beta_r = 2.8) \tag{13}$$

As shown in the figures, the values of $(l/l_0)_r$ and $(l/l_0)_c$ are almost linear with $Ri_r$ and $Ri_c$ for the rotational speed $N=0.15$ when $-0.2 < Ri_r < 0$ and $0 < Ri_c < 0.2$. Except for this rotation number, the linearity between the mixing length and two Richardson numbers is seen to be poor. For the negative values of $N$, turbulence is largely suppressed by the wall curvature, and the stabilizing effect due to the channel rotation for $N=$

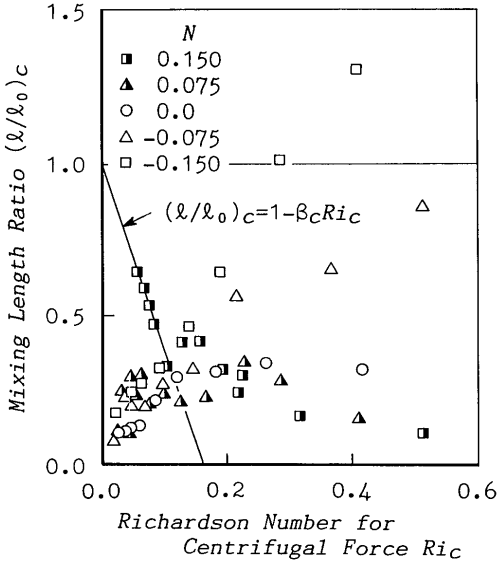


Fig. 13(a) Plots of mixing length $(l/l_0)_c$ versus Richardson number $Ri_c$ due to wall curvature

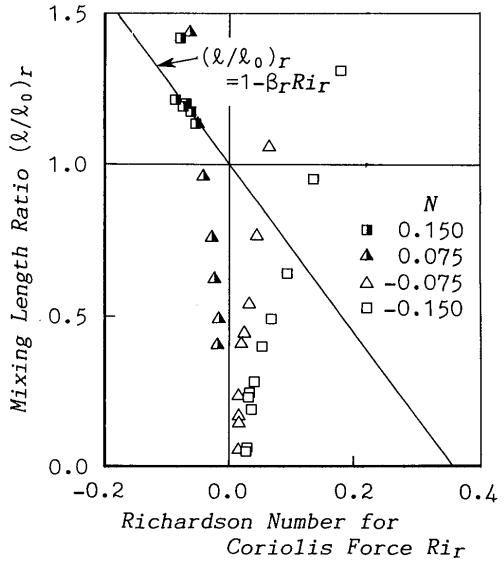


Fig. 13(b) Plots of mixing length $(l/l_0)_r$ versus Richardson number $Ri_r$ due to system rotation

$-0.075$ and $-0.15$ is seen to be less. Values of $\beta_r=2.8$ and $\beta_c=6.1$ obtained for the flows of the positive rotation number $N$ in this experiment, however, seem to be a little smaller than those proposed by Johnston for a rotating flat surface ($\beta_r=4\sim8$) and those by Bradshaw for a convex surface ($\beta_c=7\sim10$).

## 6. Conclusions

By the use of a rotating two-dimensional curved channel whose convex-surface curvature is $R/D=6.17$ and aspect ratio is 4, the behavior of the flow and turbulent fluctuations on a convex surface were examined experimentally. The results are summarized as follows.

(1) The turbulence in the boundary layer along the convex surface is suppressed in the downstream direction due to the stabilizing effects of the centrifugal force caused by wall curvature. As stabilization increases on the suction side due to the Coriolis force generated by channel rotation, the flow has a tendency to become laminarized.

(2) On the pressure side the turbulence intensities are increased and the destabilizing effects due to channel rotation exceed the stabilizing effects due to the centrifugal force.

(3) The linear Monin-Oboukhov formula is not valid for the boundary layer on a rotating convex surface since the effects of the centrifugal force due to the wall curvature become dominant on the surface.

## Acknowledgements

The authors wish to express their appreciation to Mr. H. Murakami and Mr. H. Kanda for their assistance in the experiment.

## References

(1) Koyama, H., Masuda, S., Ariga, I. and Watanabe, I., Stabilizing and Destabilizing Effects of Coriolis Force on Two-Dimensional Laminar and Turbulent Boundary Layers, Trans. ASME, J. Eng. Power, Vol. 101, No. 1, (1979), p. 23.

(2) Kikuyama, K., Murakami, M., Oshiro, M., Adachi, M., Hara, S. and Lee, K., Effects of Coriolis Force on the Turbulent Boundary Layer with Pressure Gradients, Trans. Jpn. Soc. Mech. Eng., (in Japanese), Vol. 51, No. 472, B (1985), p. 4162.

(3) Ramaprian, B. R. and Shivarasad, B. G., The Structure of Turbulent Boundary Layers along Curved Surfaces, J. Fluid Mech., Vol. 85, Part 2 (1978), p. 273.

(4) Johnston, J. P. and Eide, S. A., Turbulent Boundary Layer on Centrifugal Compressor Blades, Trans. ASME., J. Fluids Engng., Vol. 98, Series 1, (1976), p. 374.

(5) Kikuyama, K., Nishibori, K., Hara, S. and Murakami, M., Effects of Channel Rotation upon Turbulent Boundary Layer on a Concave Surface, Trans. Jpn. Soc. Mech. Eng., (in Japanese), Vol. 53, No. 492, B (1987), p. 2357.

(6) Bradshaw, P., The Analogy between Streamline Curvature and Buoyancy in Turbulent Shear Flow, J. Fluid Mech., Vol. 36, Part 1 (1969), p. 177.

(7) Johnston, J. P., Suppression of Shear Layer Turbulence in Rotating Systems, Trans. ASME, J. Fluids Eng., Vol. 95, No. 6, (1973), p. 229.